University of Texas Rio Grande Valley

ScholarWorks @ UTRGV

Mechanical Engineering Faculty Publications and Presentations

College of Engineering and Computer Science

2-2020

Hybrid phase-change Lattice Boltzmann simulation of vapor condensation on vertical subcooled walls

Wandong Zhao
Nanchang University

Yuan Gao
West Virginia University

Ruijie Li
West Virginia University

Songgang Qiu
West Virginia University

Yin Zhang
Nanchang University

See next page for additional authors

Follow this and additional works at: https://scholarworks.utrgv.edu/me_fac

Part of the Mechanical Engineering Commons

Recommended Citation

Authors

Wandong Zhao, Yuan Gao, Ruijie Li, Songgang Qiu, Yin Zhang, and Ben Xu

Hybrid phase-change Lattice Boltzmann simulation of vapor condensation on vertical subcooled walls

Wandong Zhao[1,2], Yuan Gao[2], Ruijie Li[2], Songgang Qiu[2], Ying Zhang[1*], Ben Xu[3*]

1. School of Mechanical and Electrical Engineering, Nanchang University, Nanchang, Jiangxi, 330031, China

2. Department of Mechanical and Aerospace Engineering, West Virginia University, Morgantown, WV 26506, USA

3. Department of Mechanical Engineering, University of Texas Rio Grande Valley, Edinburg, TX, 78539, USA

*Corresponding author

Tel: +86 79183969634; Email: yzhan@ncu.edu.cn (Ying Zhang)

Tel: +1 (956)665 -2896; Email: ben.xu@utrgv.edu (Ben Xu)

Abstract:

Saturated vapor condensation on homogenous and heterogeneous subcooled walls is presented in this study by adopting a hybrid phase-change multiple-relaxation-time Lattice Boltzmann model. The effects of wall wettability on the condensation process, including droplets' growth, coalescence and falling, and the influence of vapor flow to condensation are investigated. The results demonstrate that the heat fluxes around the triple-phase contact lines are higher than that in other cold areas in homogeneous subcooled walls, which actually indicates the fact that filmwise condensation is preventing the continuous condensation process. Furthermore, the dropwise condensation can be formed more easily on the heterogeneous surface with a mixed surface wettability. At last, the dynamic process of condensation of continuous vapor flow is also investigated by considering the homogenous and heterogeneous subcooled surfaces. The results show that the heterogeneous surface with mixed wettability doesn't contribute to the formation, growth of droplets, when compared to the homogeneous surface. It is expected that this study can bring more attentions to simulate condensation using multiphase LBM for complex geometries in heat transfer community.

Keywords:

Vapor condensation; Pseudopotential phase-change model; Lattice Boltzmann method (LBM); Homogenous and heterogeneous wall; Continuous-flow vapor condensation

1. Introduction

Condensation in the form of liquid-gas phase change is a complicated and interesting physical heat transfer process, which can be found in many natural phenomena [1, 2], industrial applications and manufacturing processes [2-6]. Over the past decades, a lot of researches have been conducted on the mechanism and enhancement of vapor condensation through experimental study and numerical simulation [7-9], in order to improve the heat transfer efficiency [5]. However, because of the nature of numerical simulation, more detailed condensation process can be revealed by controlling various parameters. Li [10] adopted a Computational Fluid Dynamic (CFD) tool to simulate the steam condensation with different qualities in coolant channels, which

considerably limit the heat transfer of steam vapor, because the average axial velocity drops significantly as the vapor condensing. Riva and Col [11] discussed the film condensation in a mini-channel using the Volume of Fluid (VOF) method, and reported that the film thickness becomes thicker from the inlet to the outlet. More investigations of vapor condensation conducted by CFD can be found in Refs. [12, 13].

Recently, the pseudopotential multiphase lattice Boltzmann (LB) method, due to its capability of self-generating the two-phase interface and no special requirement to treat the two-phase interface, has been extensively applied in multiphase flow simulation [14, 15]. In addition, when the energy equation was added into the pseudopotential LB model, which resulted in a series of phase change LB models. For example, Zhang and Chen [16] proposed the first liquid-vapor Phase Change LB Model (PCLBM) based on the diffusion interface energy equation. Gong and Cheng [17, 18] also developed an improved double-distribution single-relaxation-time (SRT) PCLBM. Liu and Cheng [19] investigated the film condensation on the vertical subcooled surface using the same double-distribution SRT PCLBM, and this model was also employed to simulate the dropwise condensation on a hydrophobic surface [17, 18]. Most recently, based on the same model. Li and Cheng [20] performed a numerical simulation on the saturated steam condensation on a heterogeneous surface. However, since the Bhatanagar-Gross-Krook collision operator as employed to solve the phase change in the double-distribution SRT PCLBM [17], the numerical stability and the selection of the fluid properties are slightly limited [21]. Some scholars [22, 23] also found that the double-distributions PCLBM cannot be completely recovered to the macroscopic energy conservation equation, therefore PCLBM coupled with the finite-difference method (FDM) was proposed to solve the temperature field. Li et al. [24] proposed a hybrid thermal PCLBM incorporated FDM in the original Shan-Chen's [25] pseudopotential model, and they successfully simulated the nucleate and film boiling via the hybrid PCLBM [24]. In addition, the self-driving phenomenon of droplet falling on a hot serrated surface [26] and the droplet evaporation on the heterogeneous surface [27] were investigated by using the same model.

However, vapor condensation has not been studied using the hybrid PCLBM model, most of the works are for boiling heat transfer. In addition, it was found that there are few studies addressing the dynamic behaviors and mechanism of saturated vapor condensation on a vertical subcooled surface, and the flow boundary conditions for the condensed liquid are difficult to be realized in the model. For this reason, this work is aimed to investigate the dynamic process of vapor condensation on the vertical subcooled walls using the hybrid phase change LBM model. It is expected that this study can bring more attentions to simulate condensation using multiphase LBM for complex geometries in heat transfer community.

2. Numerical model

The hybrid PCLBM developed by Li. *et al* [24] was used in this work, and it will be briefly discussed in this section. The derivation of diffusion energy governing equation will be introduced in detail. The flow evolution of density distribution function (DF) of MRT collision is given by [24]

$$f_\alpha(\boldsymbol{x} + \boldsymbol{e}_\alpha \delta_t, t + \delta_t) = f_\alpha(\boldsymbol{x}, t) - (\boldsymbol{M}^{-1} \boldsymbol{\Lambda} \boldsymbol{M})_{\alpha\beta} (f_\beta - f_\beta^{eq})\big|_{(x,t)} + \delta_t F_\alpha' \qquad (1)$$

where δ_x and δ_t are the lattice space and time step, and both were set to 1, so $c = \delta_x / \delta_t = 1$ [28]. With the transfer matrix $\boldsymbol{M}$, the right side of (1) can be further obtained as [29]

$$m^* = m - \Lambda(m - m^{eq}) + \delta_t(I - \frac{\Lambda}{2})\overline{S} \tag{2}$$

where $\overline{S} = MS$ is the external forcing term, and $S = (S_0, S_1, S_2, S_3, S_4, S_5, S_6, S_7, S_8)^T$.

The fluid-fluid interaction force for the single-component (SC) multiphase model can be shown as [30]

$$F_m = -G\psi(x,t)\left[\sum_i w(|e_\alpha|^2)\psi(x + e_\alpha, t)e_\alpha\right] \tag{3}$$

where the weights factors are $w(1) = 1/3$ and $w(2) = 1/12$, and ψ in (3) can be defined as [31]

$$\psi = \sqrt{\frac{2(P_{EOS} - \rho c_s^2)}{Gc^2}} \tag{4}$$

where EOS denotes the equation of state.

The EOS developed by Peng & Laura [32] by considering the diffusion interface was applied. At the same time, a new solid-fluid interaction force proposed by Li $et.$ al [31, 33] was utilized to include the wettability characteristic in the model,

$$F_{ads} = -G_w\psi(x)\left[\sum_i w(|e_\alpha|^2)\psi(x)S(x + e_\alpha)e_\alpha\right] \tag{5}$$

The gravitational force F_g is determined as $F_g(x) = (\rho(x) - \rho_v)g$, therefore the total force can be defined as $F = F_m + F_{ads} + F_g$.

The liquid-vapor PCLB model based on the diffusion interface was first proposed by Zhang & Chen [16],

$$\rho\frac{De}{Dt} = -p\nabla \cdot \mathbf{v} + \nabla \cdot (\lambda\nabla T) \tag{6}$$

The entropy's local equilibrium energy equation can be shown as follows by neglecting viscous dissipation

$$\rho T\frac{Ds}{Dt} = \nabla \cdot (\lambda\nabla T) \tag{7}$$

According to the Maxwell equations, we can obtain the following one,

$$ds = \frac{C_V}{T}dT + \left(\frac{\partial p}{\partial t}\right)_V dv = \frac{C_V}{T}dT + \left(\frac{\partial p}{\partial t}\right)_V d\left(\frac{1}{\rho}\right) = \frac{C_V}{T}dT - \frac{1}{\rho^2}\left(\frac{\partial p}{\partial t}\right)_V d\rho \tag{8}$$

By substituting Eq. (8) into Eq. (7), it can be rewritten as

$$\rho C_V\frac{DT}{Dt} = \frac{T}{\rho}\left(\frac{\partial p}{\partial t}\right)_\rho\frac{d\rho}{dt} + \nabla \cdot (\lambda\nabla T) \tag{9}$$

Therefore using the material derivative $D(\ )/Dt = \partial_t(\ ) + \mathbf{v} \cdot \nabla(\ )$, Eq. (9) can be converted to

$$\frac{\partial T}{\partial t} = -\mathbf{v} \cdot \nabla T + \frac{1}{\rho C_V}\nabla \cdot (\lambda\nabla T) + \frac{T}{\rho^2 C_V}\left(\frac{\partial p}{\partial t}\right)_\rho\frac{d\rho}{dt} \tag{10}$$

Eq. (10) can further be rewritten as [24]

$$\frac{\partial T}{\partial t} = -\mathbf{v} \cdot \nabla T + \frac{1}{\rho C_V}\nabla \cdot (\lambda\nabla T) - \frac{T}{\rho C_V}\left(\frac{\partial p}{\partial t}\right)_\rho\nabla \cdot \mathbf{v} \tag{11}$$

To numerically solve Eq. (11), the diffusion term is discretized by the central difference scheme. As for the time derivative, we tested both the 2nd order and 4th order Runge-Kutta methods for the phase-change process,

and it was found that some unsymmetric results appeared if the 2nd order Runge-Kutta method was used. This phenomenon is probably due to the fact that LBM model has a high sensitivity for dealing with phase-change process, even though this high-order scheme cannot realize the expected time resolution, it did help remove the unsymmetric results. Consequently, to avoid these unsymmetric results, the 4th order Runge-Kutta method [24] was chosen in this work. If we mark the right side of Eq. (11) as $K(T)$, so Eq. (11) can be discretized as,

$$T^{t+\delta t} = T^t + \frac{\delta t}{2}(h_1 + h_2 + h_3 + h_4)$$ (12)

$$h_1 = K(T^t), h_2 = K(T^t + \frac{\delta_t}{2}h_1), h_3 = K(T^t + \frac{\delta_t}{2}h_2), h_4 = K(T^t + \delta_t h_3)$$ (13)

For a quantity ϕ, the gradient and Laplace operator are calculated by [35]

$$\partial_i \phi(\boldsymbol{x}) \approx \frac{1}{c_s^2 \delta_t}\left[\sum_a w_\alpha \phi(\boldsymbol{x} + \boldsymbol{e}_a \delta_t)\boldsymbol{e}_a\right]$$ (14)

$$\nabla^2 \phi(\boldsymbol{x}) \approx \frac{2}{c_s^2 \delta_t^2}\left[\sum_a w_\alpha (\phi(\boldsymbol{x} + \boldsymbol{e}_a \delta_t) - \phi(\boldsymbol{x}))\right]$$ (15)

3. Results and discussion

It is worth noting that the hybrid thermal PCLBM was verified by simulating the droplet evaporation, which has a good agreement with the D^2 law [26, 36, 37]. In this section, numerical simulations about saturated vapor condensation on vertical subcooled homogeneous/ heterogeneous surfaces with various wetting characteristics were studied by adopting the hybrid thermal PCLBM model, the results will be discussed in detail as follows.

3.1. Computational domain and boundary conditions

Three different numerical models were developed in this study, and the computational domain and boundary conditions can be found in Fig. 1, in which the computational domains are divided into three sections for all three cases, and the top and bottom parts with red boundaries are the adiabatic walls, while in the middle part, Models A and C have a homogeneous wettability characteristic (hydrophobic wall with lower temperature), and Models B and D shows heterogeneous wettability characteristic (segregated hydrophobic and hydrophilic wall with lower temperature). Fig. 2 illustrates the heterogeneous wall of Model B, in which the yellow parts represent the hydrophilic regions, and the blue areas indicate the hydrophobic surfaces. The length of hydrophilic and hydrophobic regions are marked by L_s and L_w, respectively. The top and bottom boundary conditions for Model A and B are periodic, the half-way bounce back boundary condition [38] for density DF is employed on the solid wall, and the entire computational domain is full with the started vapor, in addition the gravitational force is applied. However, in order to investigate the effect of vapor flow to condensation on hydrophobic surface, Models C and D are introduced in Fig. 1, where the non-equilibrium extrapolation boundary condition [39] is adopted for the velocity inlet, and the outflow boundary condition [40] is chosen for the Models C and D.
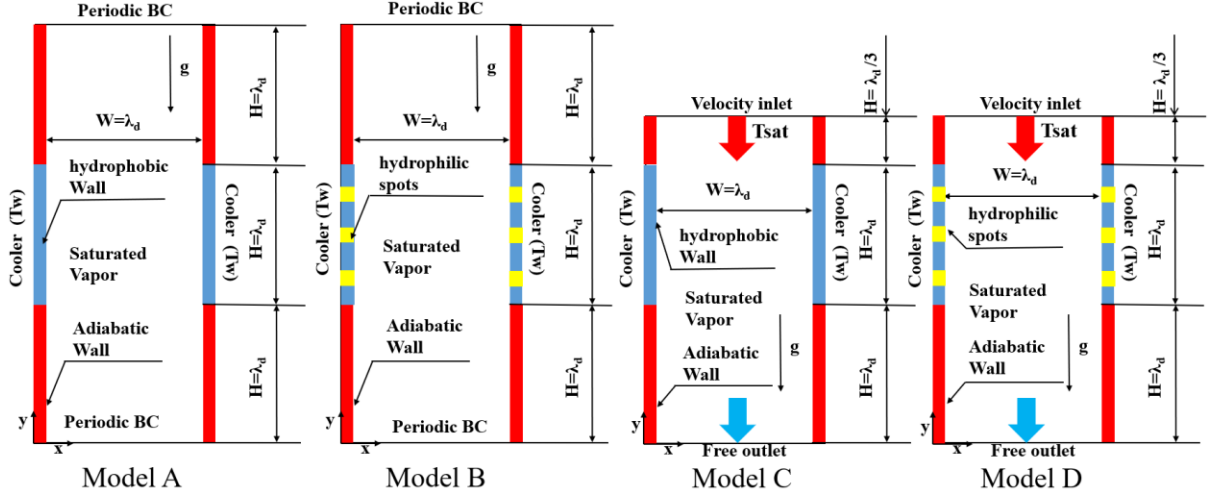
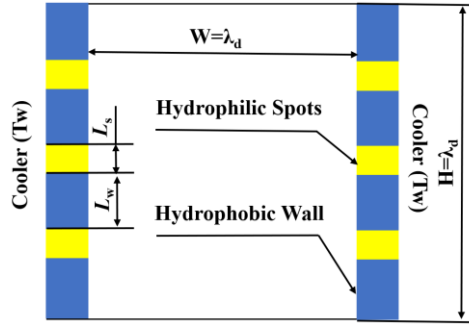Fig. 1. Schematic of physical model for vapor condensation.

Fig. 2. Schematic of the heterogeneonous subcooled surface.

The degree of wall subcooling can be quantified using Jacob number in (23) [20].

$$Ja = \frac{c_v (T_{sat} - T_w)}{h_{fg}} \quad (16)$$

where h_{fg} is the latent heat [17, 18], c_v is the specific heat capacity, T_{sat} is the saturated temperature, and T_w is the wall temperature. Since h_{fg} was chosen as 0.58, therefore Ja number was 0.33 in this study.

In order to nondimensionalize the governing equations, following the definitions in Ref. [20], the characteristic length can be defined as

$$l_0 = \sqrt{\frac{\sigma}{g(\rho_l - \rho_v)}} \quad (17)$$

where σ is the surface tension, ρ_l is the liquid phase density, and ρ_v is the vapor phase density.

The characteristic time can be evaluated by (18).

$$t_0 = \sqrt{l_0 / g} \quad (18)$$

Since all the physical parameters were based on the lattice units. Table 1 lists the values of different cases. The saturated temperature is $T_{sat} = 0.86 T_{cr}$, and T_{cr} is the critical temperature, equal to 0.1094 in this study. Therefore, the densities of liquid and gas phases are $\rho_l = 6.5$, $\rho_g = 0.38$, respectively. It is important to mention

that we didn't consider the case when θ_w =155º and θ_s =65º, because the 90º difference of contact angle cannot lead to converged results, we will make more efforts on the contact angle by improving the G_w modeling in (5) as future work.

Table 1. Parameters of different cases adopted in this work

Case	θ_s	θ_w	Ja	$L_s* = L_s / l_0$	$L_w* = L_w / l_0$	# of hydrophilic spots
1	-	115°	0.33	-	-	-
2	-	135°	0.33	-	-	-
3	-	155°	0.33	-	-	-
4	65°	115°	0.33	0.33	3.90	3
5	65°	135°	0.33	0.33	3.90	3

Note that θ_s and θ_w denote the hydrophilic and hydrophobic surface, respectively.

3.2. Saturated vapor condensation on homogeneous and heterogeneous walls

3.2.1. Dynamic process of condensation and phase contour

The dynamic processes of vapor condensation on subcooled walls with hydrophobic surface (θ_w =115°) are shown in Fig. 3. A high degree of subcooling (Ja =0.33) was chosen to reveal the effect of wettability on the vapor condensation. In Fig. 3, the red and blue colors represent the condensate droplets and the saturated vapor, respectively. When t*=6.67, a thin liquid film is formed in the middle part of the computational domain, and several separated and tiny droplets can be observed. When t*=11.68, the liquid film becomes thicker and aggregates at the middle part of the two side walls due to the effect of gravity and surface tension. Meanwhile, lots of small droplets grow in the middle regions as shown in Fig. 3 (c). When t*=20.02, the surrounding droplets gradually grow in volume and coalesce small condensate droplets, resulting in the rapid growth of large droplets. The droplets begin to fall along the cooler surface under the effects of gravity, and the contact angle hysteresis could be clearly observed as indicated in Fig. 3 (f).
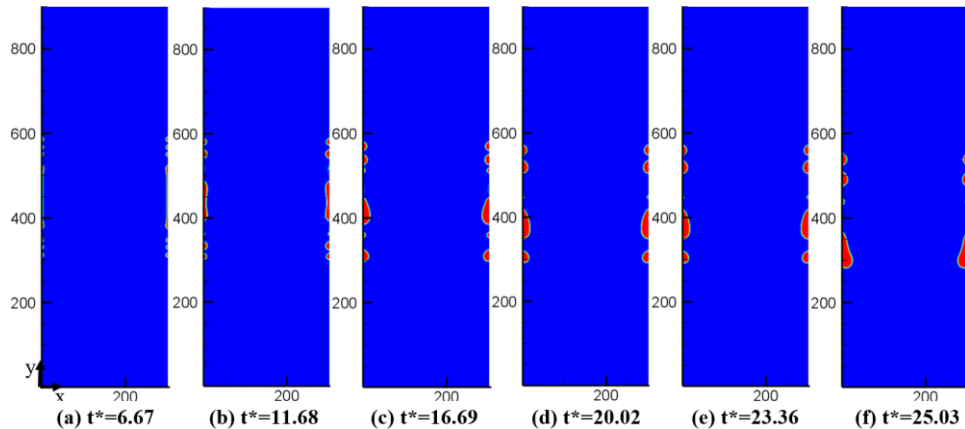

Fig. 3. Snapshots of vapor condensation under the homogeneous hydrophobic subcooled wall (Case #1).

Fig. 4 illustrates the phase contour for Case # 2 when the contact angle is 135º. As shown in Fig. 4, when t*=6.67, it is similar with Case #1, but the liquid film is thinner and the droplet is smaller in Case #2. At t*=11.68,

6

there is a big droplet in the middle by accumulating its surrounding tiny droplets, due to the decrease of wetting and a lower wall adhesion, but Case #1 takes longer time to form a big droplet in the middle area of the wall. Furthermore, the liquid film shrinks quickly under the surface tension effect. At t*=16.69, the volumes of droplets are greater than the droplets in Case #1 at the same time instant. As indicated by Fig. 4 (c), (d), (e) and (f), the droplet at Y=400 starts to merge other droplets underneath, and eventually there is only one big droplet which forms at Y=300 in Fig. 4 (e), and it continues to move downward following its preset hydrophobic contact angle, as shown in Fig. 4 (f).
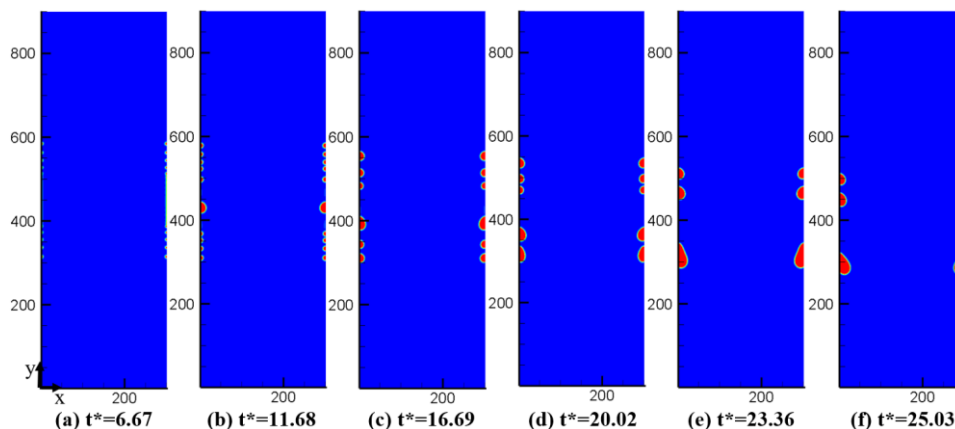

Fig. 4. Snapshots of saturated vapor condensation characteristics (Case #2).

Similarly, when the contact angle was changed to 155º, the surface wettability became super-hydrophobic, as indicated in Table 1. Fig. 5 shows the phase contour of vapor condensation at different instants. Obviously, the liquid film is almost negligible at t*=6.67, and there are much more tiny droplets generated when t*=11.68 and t*=16.69. Furthermore, there is a significant delay of droplet merging, due to the super-hydrophobic surface, as indicated in Fig. 5 (d) and (e).
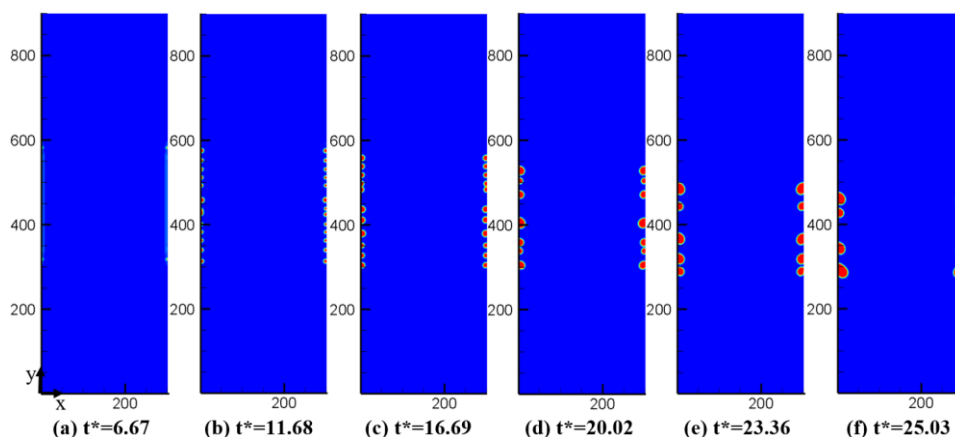

Fig. 5. Time evolutions of vapor condensation process on super-hydrophobic subcooled surface (Case #3).

From Fig. 5, we can find that there are more large droplets existed on the super-hydrophobic wall, in other words the super-hydrophobicity can prevent the formation of film condensation, but the initial stage for Case #1, #2 and #3 has a high potential to form film condensation due to the existence of many tiny droplets, and it will

7

further deteriorate the formation of droplets. Therefore, instead of having the same wettability for the subcooled wall, we propose to adopt a mixed surface wettability for the subcooled wall.

Therefore, the effect of mixed surface wetting characteristic on vapor condensation was also investigated, as shown in Figs. 6 and 7, which corresponds to Case #4 and Case #5 in Table. 1. From Figs. 6 (a) and 7 (a), there are many tiny and isolated droplets growing on the heterogeneous wall at the same time, rather than forming a thin liquid film in the middle region as in Fig. 3 (a), so adopting the mixed surface wettability can significantly promote the formation of dropwise condensation. Droplets keep growing up ($t*$=10.01 and $t*$=13.35) and some droplets begin to coalesce at $t*$=16.69. Finally, some droplets start to fall along the vertical wall due to gravity, as shown in Figs. 6 & 7 (e & f). Furthermore, it is also found that the dynamic process of vapor condensation in Cases #4 and #5 are very similar, so increasing the contact angle of hydrophobic surface has a negligible effect to form the dropwise condensation. Nevertheless, when the contact angle is further increased to 155º, converged simulation results cannot be obtained, therefore it implies that the modeling of G_w in (5) need to be further improved in our future study.
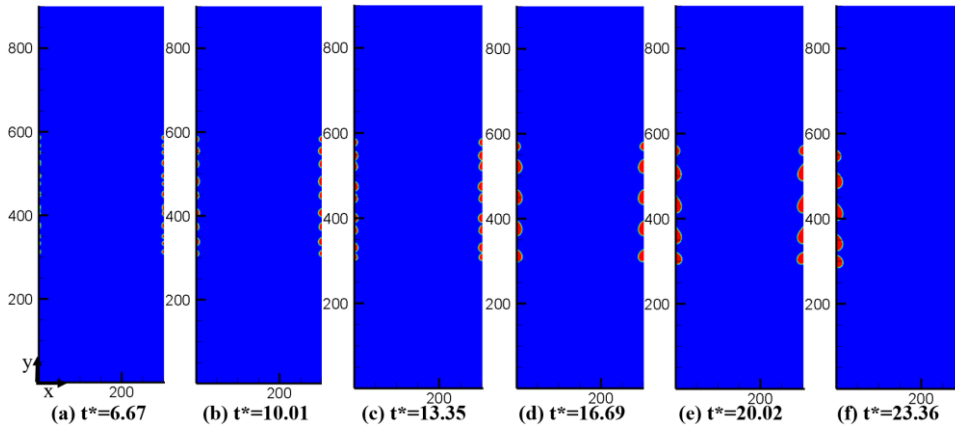

Fig. 6. Snapshots of vapor condensation on the heterogeneous subcooled surface (Case 4#).
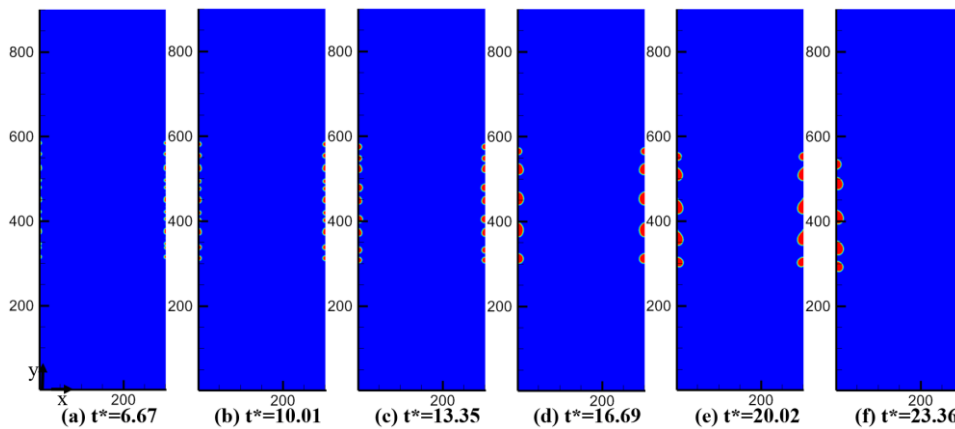

Fig. 7. Snapshots of vapor condensation on the heterogeneous subcooled surface (Case 5#).

3.2.2. Temperature contour and local heat flux

Following Ref. [20], the local heat flux can be evaluated by

$$q^*(x, y, t) = \frac{(-\lambda \,\partial T/\partial y)}{q_0} = \frac{1}{\rho_l \upsilon_l h_{fg}} \sqrt{\frac{\sigma}{g(\rho_l - \rho_g)}} (-\lambda \frac{\partial T}{\partial y}) \bigg|_{x=0} \qquad (19)$$

where $q_0 = \mu_l h_{fg} \sqrt{g(\rho_l - \rho_g)/\sigma}$ is the reference heat flux, and q_0^{lu} is assumed as 0.02099. The gradient of temperature is calculated by

$$\frac{\partial T}{\partial y} = \frac{4T\big|_{(x,1)} - T\big|_{(x,2)} - 3T\big|_{(x,0)}}{2\delta_y} \qquad (20)$$

Fig. 8 demonstrates the non-dimensional temperature field ($T^* = T/T_{cr}$) at t*=11.68 for Cases #1, #2, #4 and #5, where the black line in the figures indicates the liquid-vapor interface. As shown in Fig. 8, for Case #3, there is a higher temperature region in the middle of computational domain compared to Cases #1, #2 and #5. This is because the vapor condensation ratio is low by introducing the hydrophilic surface with 65° contact angle. We also can observe from Fig. 8 that the areas above all the droplets have higher temperatures, which is due to the heat released from condensation. However, Case #1 in Fig. 8 has much larger areas with higher temperatures, which may be caused by the formation of thermal resistance which suppresses the heat transfer from the cold wall to vapor, in other words the filmwise condensation cannot produce a high heat transfer efficiency. Furthermore, the temperature contour is much more crowded in the triple-phase contact lines than that in other areas where no phase change is occurring, which has been confirmed by Ref. [20].
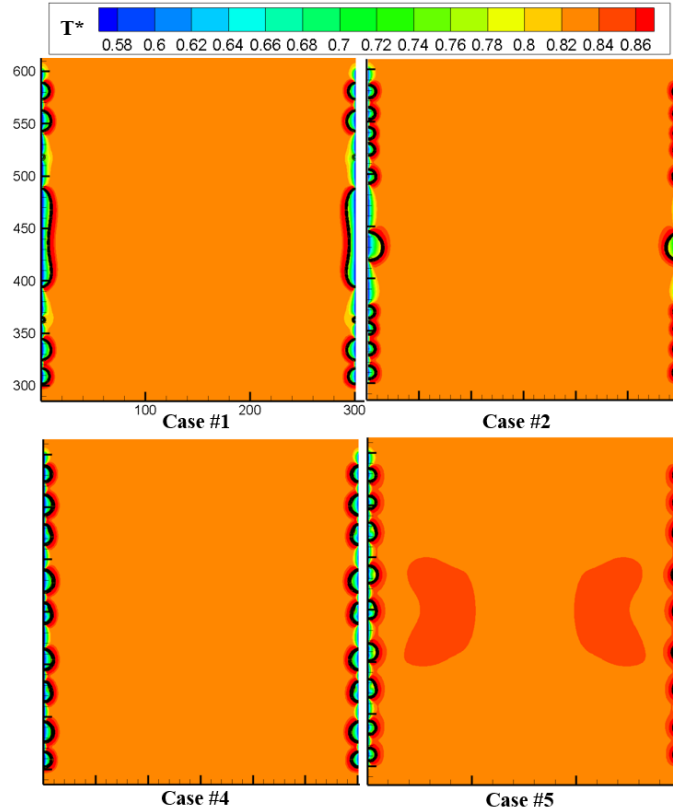

Fig. 8. The dimensionless temperature field at t*=11.68 in the region of ($0 < Nx < 300, 300 < Ny < 600$) for Cases #1-4).

In order to explore the difference of heat flux between homogeneous and heterogeneous walls, Fig. 9 demonstrates the comparison of local heat flux distributions between Case #1 and #3, Case #2 and #5 at t^*=6.67. From Fig. 9, the heat fluxes of Case #4 and #5 vary in a broad range with a relative uniform and higher value than Case #1 and #2, whereas the heat flux is almost remained as a constant for the homogeneous wall due to the appearance of filmwise condensation in the middle region 0.45<Y/Ny<0.55. Consequently, at the initial stage of condensation, dropwise condensation can easily be formed on the heterogeneous wall compared to the homogenous wall.
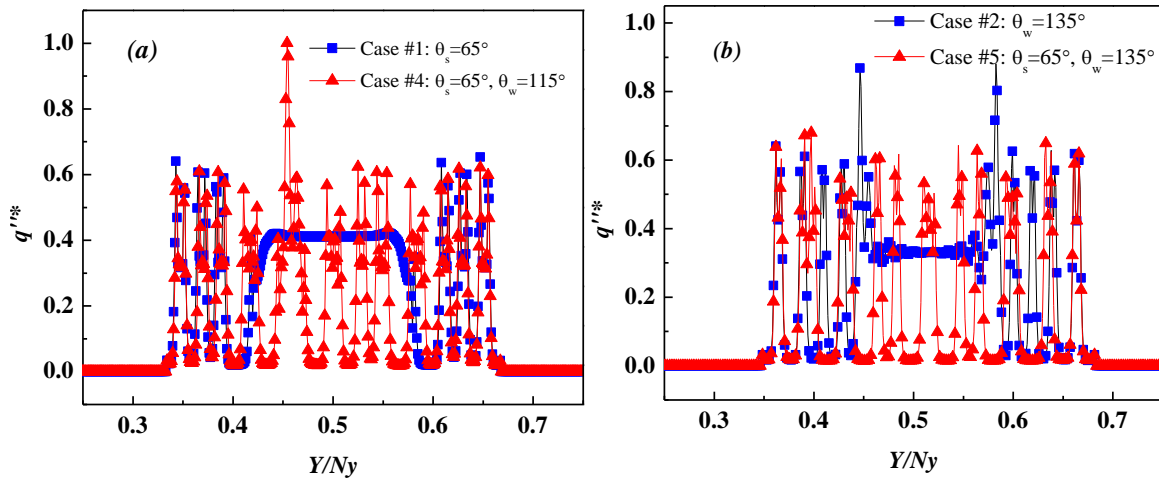

Fig. 9. Comparison of local heat flux on the homogenous and heterogeneous wall at t^*=6.67.

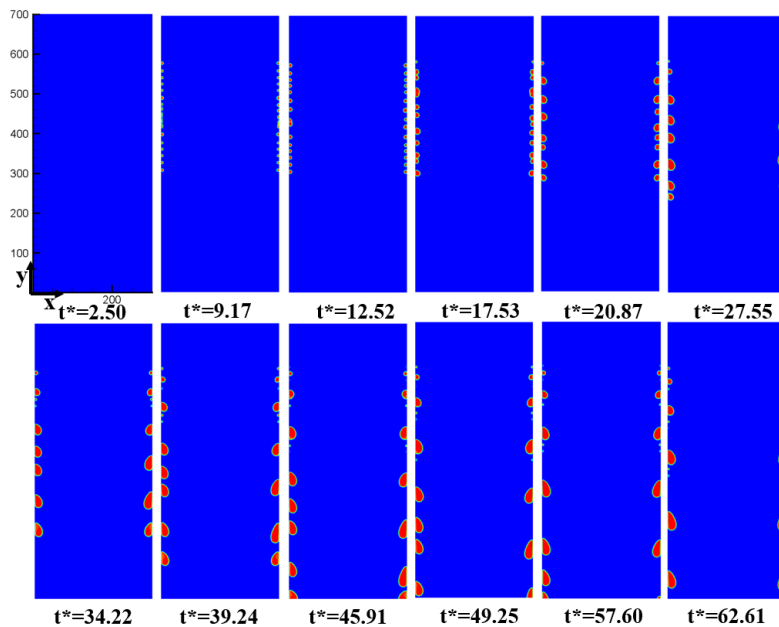### 3.3. The effect of flow to the vapor condensation on homogeneous hydrophobic walls

Fig. 10 Snapshots of condensation of continuous-flow vapor under the homogeneous hydrophobic subcooled wall (Case #1).

Model A and Model B in Fig. 1 are for the condensation process of stationary saturated vapor in previous two

sections, to further explore the effect of vapor flow to condensation, we chose Model C by incorporating the fully developed flow as the inlet boundary condition. It is important to mention that the condensation in continuous flow condition is extremely difficult due to the need of special treatment of boundaries, but the hybrid phase-change LBM model can successfully be implemented. In the simulation, the maximum inlet velocity (downward) is set as 0.02, while other boundary conditions are remained the same as Case #1 in Table 1 so that the contact angle of the subcooled surface is 115º. Fig. 10 shows the phase contour of liquid condensate at various instants during the condensation process. Compared with Fig. 3, the continuous vapor flow delays the occurrence of condensation, and also prevents the formation of filmwise condensation. Furthermore, the condensate droplets can continuously fall off from the subcooled walls under the effect of gravity, and the falling droplets have almost the same size before they move out from the computational domain. Based on the maximum velocity at the inlet, the Reynolds number is 60 if the width between two subcooled walls is used as the characteristic length. Apparently, the flow is in laminar regime, and no strong disturbance can be generated to affect the falling of droplets, therefore the condensate droplets can maintain relatively the same size at the exit of domain.

It is also interesting to compare Case #1 under continuous vapor flow with Case #4, so the effect of mixed wetting characteristics on condensation can be compared with the homogeneous subcooled surface. The simulated resulted can be found in Fig. 11. Apparently, Fig. 10 and Fig. 11 have not much differences in terms of the number of droplets and droplet size at the exit of computational domain, therefore we can conclude that in terms of the boundary conditions described in Table 1, the mixed wettability surface under continuous flow doesn't contribute to the droplet formation, merging and growth, when compared with the homogeneous subcooled walls.
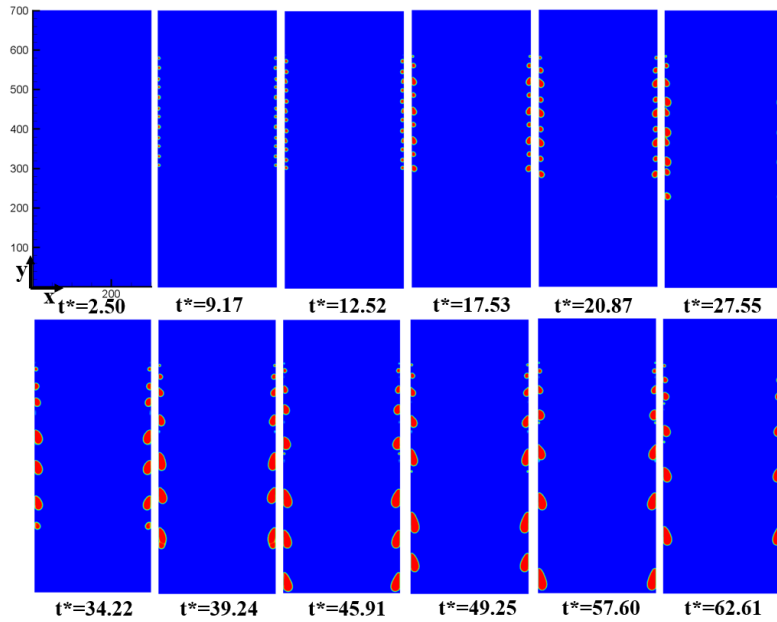

Fig. 11 Snapshots of condensation of continuous-flow vapor under the homogeneous hydrophobic subcooled wall (Case #4).

4. Conclusions

In this work, we adopt the hybrid PCLBM to simulate stationary and flowing vapor condensation on the vertical subcooled walls, and the dynamic condensation process is discussed by varying the surface wettability.

Some key conclusions are listed as follows:

a) Decreasing the surface wettability is easy to yield dropwise condensation;

b) High condensation heat fluxes appear near the triple-phase contact line;

c) The subcooled surface with mixed wettability is easier to form dropwise condensation than the homogeneous wall, but it does not have significant effect on vapor condensation if compared to the homogenous surface.

Reference

[1] Segal, Y., Khain, A., Pinsky, M., and Sterkin, A., 2010, "Sensitivity of raindrop formation in ascending cloud parcels to cloud condensation nuclei and thermodynamic conditions," Quarterly Journal of the Royal Meteorological Society, 130(597), pp. 561-581.

[2] Kandlikar, S. G., 1999, "Handbook of Phase Change: Boiling and Condensation," Multiphase Flow Handbook.

[3] Chaudhry, H. N., Hughes, B. R., and Ghani, S. A., 2012, "A review of heat pipe systems for heat recovery and renewable energy applications," Renewable & Sustainable Energy Reviews, 16(4), pp. 2249-2259.

[4] Kuo, W. S., Lie, Y. M., Hsieh, Y. Y., and Lin, T. F., 2005, "Condensation heat transfer and pressure drop of refrigerant R-410A flow in a vertical plate heat exchanger," International Journal of Heat & Mass Transfer, 48(25–26), pp. 5205-5220.

[5] Dalkilic, A. S., and Wongwises, S., 2009, "Intensive literature review of condensation inside smooth and enhanced tubes," International Journal of Heat & Mass Transfer, 52(15–16), pp. 3409-3426.

[6] Ma, M., Lu, J., and Tryggvason, G., 2015, "Using statistical learning to close two-fluid multiphase flow equations for a simple bubbly system," Physics of Fluids, 27(9), p. 092101.

[7] Li, W., Zhang, J., Bai, G., Xu, J.-l., Simon, T. W., Li, J., and Wei, J.-j., 2016, "Numerical Simulation of Condensation for R410A in Horizontal Round and Flattened Minichannels," Journal of Heat Transfer, 139(2).

[8] Cao, H., and Li, J.-D., 2017, "Computational Fluid Dynamics Simulations of Convective Pure Vapor Condensation Inside Vertical Cylindrical Condensers," Journal of Heat Transfer, 139(6).

[9] Wróblewski, W., Dykas, S., Gardzilewicz, A., and Kolovratnik, M., "Numerical and Experimental Investigations of Steam Condensation in LP Part of a Large Power Turbine," Journal of Fluids Engineering, 131(4), p. 041301.

[10] Li, J. D., 2013, "CFD simulation of water vapour condensation in the presence of non-condensable gas in vertical cylindrical condensers," International Journal of Heat & Mass Transfer, 57(2), p. 708.

[11] Riva, E. D., and Col, D. D., 2012, "Numerical Simulation of Laminar Liquid Film Condensation in a Horizontal Circular Minichannel," Journal of Heat Transfer, 134(5), p. 051019.

[12] Rose, J., 2002, "Dropwise condensation theory and experiment: a review," Proceedings of the Institution of Mechanical Engineers, Part A: Journal of Power and Energy, 216(2), pp. 115-128.

[13] Kharangate, C. R., and Mudawar, I., 2017, "Review of computational studies on boiling and condensation," International Journal of Heat and Mass Transfer, 108, pp. 1164-1196.

[14] Li, Q., Luo, K. H., Kang, Q. J., He, Y. L., Chen, Q., and Liu, Q., 2016, "Lattice Boltzmann methods for multiphase flow and phase-change heat transfer," Progress in Energy & Combustion Science, 52, pp. 62-105.

[15] Chen, L., Kang, Q., Mu, Y., He, Y. L., and Tao, W. Q., 2014, "A critical review of the pseudopotential multiphase lattice Boltzmann model: Methods and applications," International Journal of Heat & Mass Transfer, 76(6), pp. 210-236.

[16] Zhang, R., and Chen, H., 2003, "Lattice Boltzmann method for simulations of liquid-vapor thermal flows," Physical Review E, 67(6), p. 066711.

[17] Gong, S., and Cheng, P., 2013, "Lattice Boltzmann simulation of periodic bubble nucleation, growth and departure from a heated surface in pool boiling," International Journal of Heat & Mass Transfer, 64(3), pp. 122-132.

[18] Gong, S., and Cheng, P., 2017, "Direct numerical simulations of pool boiling curves including heater's thermal responses and the effect of vapor phase's thermal conductivity," International Communications in Heat & Mass Transfer, 87, pp. 61-71.

[19] Liu, X., and Cheng, P., 2013, "Lattice Boltzmann simulation of steady laminar film condensation on a vertical hydrophilic subcooled flat plate," International Journal of Heat & Mass Transfer, 62(1), pp. 507-514.

[20] Li, X., and Cheng, P., 2017, "Lattice Boltzmann simulations for transition from dropwise to filmwise condensation on hydrophobic surfaces with hydrophilic spots," International Journal of Heat & Mass Transfer, 110, pp. 710-722.

[21] Li-Shi Luo, P. L., 2000, "Theory of the lattice boltzmann method: dispersion, dissipation, isotropy, galilean invariance, and stability," Physical Review E Statistical Physics Plasmas Fluids & Related Interdisciplinary Topics, 61(6 Pt A), p. 6546.

[22] Li, Q., Zhou, P., and Yan, H., 2017, "Improved thermal lattice Boltzmann model for simulation of liquid-vapor phase change," Physical Review E, 96(6), p. 063303.

[23] Gan, Y., Xu, A., Zhang, G., and Succi, S., 2015, "Discrete Boltzmann modeling of multiphase flows: hydrodynamic and thermodynamic non-equilibrium effects," Soft Matter, 11(26), pp. 5336-5345.

[24] Li, Q., Kang, Q. J., Francois, M. M., He, Y. L., and Luo, K. H., 2015, "Lattice Boltzmann modeling of boiling heat transfer: The boiling curve and the effects of wettability," International Journal of Heat & Mass Transfer, 85, pp. 787-796.

[25] Shan, X., and Chen, H., 1993, "Lattice Boltzmann model for simulating flows with multiple phases and components," Phys Rev E Stat Phys Plasmas Fluids Relat Interdiscip Topics, 47(3), pp. 1815-1819.

[26] Li, Q., Kang, Q. J., Francois, M. M., and Hu, A. J., 2015, "Lattice Boltzmann modeling of self-propelled Leidenfrost droplets on ratchet surfaces," Soft Matter, 12(1), pp. 302-312.

[27] Li, Q., Zhou, P., and Yan, H., 2016, "Pinning-depinning mechanism of the contact line during evaporation on chemically patterned surfaces: A lattice Boltzmann study," Langmuir the Acs Journal of Surfaces & Colloids, 32(37), p. 9389.

[28] Zhao, W., Zhang, Y., and Xu, B., 2019, "An improved pseudopotential multi-relaxation-time lattice Boltzmann model for binary droplet collision with large density ratio," Fluid Dynamics Research, 51(2), p. 025510.

[29] Zhao, W., Zhang, Y., Xu, B., Li, P., Wang, Z., and Jiang, S., 2018, "Multiple-Relaxation-Time Lattice Boltzmann Simulation of Flow and Heat Transfer in Porous Volumetric Solar Receivers," Journal of Energy Resources Technology, 140(8), p. 082003.

[30] Shan, X., and Chen, H., 1994, "Simulation of nonideal gases and liquid-gas phase transitions by the lattice Boltzmann equation," Phys Rev E Stat Phys Plasmas Fluids Relat Interdiscip Topics, 49(4), pp. 2941-2948.

[31] Zhao, W., Zhang, Y., Shang, W., Wang, Z., Xu, B., and Jiang, S., 2019, "Simulation of droplet impacting a square solid obstacle in microchannel with different wettability by using high density ratio pseudopotential multiple-relaxation-time (MRT) lattice Boltzmann method (LBM)," Canadian Journal of Physics, 97(1), pp. 93-113.

[32] Yuan, P., and Schaefer, L., 2006, "Equations of state in a lattice Boltzmann model," Physics of Fluids, 18(4), p. 329.

[33] Li, Q., and Luo, K. H., 2013, "Achieving tunable surface tension in the pseudopotential lattice Boltzmann modeling of multiphase flows," Physical Review E Statistical Nonlinear & Soft Matter Physics, 88(5), p. 053307.

[34] Liu, H., Valocchi, A. J., Zhang, Y., and Kang, Q., 2013, "Phase-field-based lattice Boltzmann finite-difference model for simulating thermocapillary flows," Phys Rev E Stat Nonlin Soft Matter Phys, 87(1), p. 013010.

[35] Lee, T., and Lin, C.-L., 2005, "A stable discretization of the lattice Boltzmann equation for simulation of incompressible two-phase flows at high density ratio," Journal of Computational Physics, 206(1), pp. 16-47.

[36] Law, C. K., 1982, "Recent advances in droplet vaporization and combustion," Progress in Energy & Combustion Science, 8(3), pp. 171-201.

[37] Safari, H., Rahimian, M. H., and Krafczyk, M., 2013, "Extended lattice Boltzmann method for numerical simulation of thermal phase change in two-phase fluid flow," Physical Review E Statistical Nonlinear & Soft Matter Physics, 88(1), p. 013304.

[38] He, X., Zou, Q., Luo, L. S., and Dembo, M., 1997, "Analytic solutions of simple flows and analysis of nonslip boundary conditions for the lattice Boltzmann BGK model," Journal of Statistical Physics, 87(1-2), pp. 115-136.

[39] Guo, Z., Zheng, C., and Shi, B., 2002, "Non—equilibrium extrapolation method for velocity and pressure boundary conditions in the lattice Boltzmann method," Chinese Physics, 11(4), pp. 366-374.

[40] Lou, Q., Guo, Z., and Shi, B., 2013, "Evaluation of outflow boundary conditions for two-phase lattice Boltzmann equation," Physical review E, 87(6), p. 063301.

[41] Michio, Y., Kunio, H., Yasuo, M., and Motokazu, U., 1985, "Fundamental study of laminar film condensation heat transfer on a downward horizontal surface," International Journal of Heat & Mass Transfer, 28(10), pp. 1937-1944.